White Rose Research Online

eprints@whiterose.ac.uk
https://eprints.whiterose.ac.uk
Universities of Leeds, Sheffield and York

Deposited via The University of Leeds.

White Rose Research Online URL for this paper:
https://eprints.whiterose.ac.uk/id/eprint/181415/

Version: Accepted Version

Article:
Niaz, T, Imran, M and Mackie, A (2021) Improving carvacrol bioaccessibility using core–shell carrier-systems under simulated gastrointestinal digestion. Food Chemistry, 353. 129505. ISSN: 0308-8146

https://doi.org/10.1016/j.foodchem.2021.129505

© 2021, Elsevier. This manuscript version is made available under the CC-BY-NC-ND 4.0 license http://creativecommons.org/licenses/by-nc-nd/4.0/.

Reuse
This article is distributed under the terms of the Creative Commons Attribution-NonCommercial-NoDerivs (CC BY-NC-ND) licence. This licence only allows you to download this work and share it with others as long as you credit the authors, but you can't change the article in any way or use it commercially. More information and the full terms of the licence here: https://creativecommons.org/licenses/

Takedown
If you consider content in White Rose Research Online to be in breach of UK law, please notify us by emailing eprints@whiterose.ac.uk including the URL of the record and the reason for the withdrawal request.

UNIVERSITY OF LEEDS
University of Sheffield
UNIVERSITY of York

Improving carvacrol bioaccessibility using core–shell carrier-systems under simulated gastrointestinal digestion

Taskeen Niaz[a,b,1], Muhammad Imran[a,*], Alan Mackie[b,*]

[a] Department of Biosciences, COMSATS University Islamabad (CUI), Park Road, Islamabad, Pakistan
[b] Food Colloids and Bioprocessing Group, School of Food Science and Nutrition, University of Leeds, Leeds LS2 9JT, UK
[1] Present Address: Pakistan Institute of Rehabilitation Sciences (PIRS), ISRA University Islamabad campus, Islamabad, Pakistan.

Abstract

The impact of encapsulating carvacrol in chitosan-albumin based core–shell nano-carriers (NCs) on its stability and bioaccessibility was determined under simulated digestion conditions. These NCs consisted of chitosan (C) core enclosed by bovine serum albumin (BSA) shell. The mean particle size ranged from 52.4 ±10 nm to 203 ±6 nm and zeta-potential from +21 ±3.6 to –18 ±2.7 mV. The size and charge were significantly modified after the protein-shell formation around the polysaccharide-core. Core-shell NCs were more stable, with less aggregation under simulated gastrointestinal conditions than C-NCs, presumably due to greater steric repulsion. Likewise, core–shell NCs were observed relatively more stabilized in the intestinal phase than gastric phase. The bioaccessibility of carvacrol was enhanced significantly when it was encapsulated in the core–shell NCs. These findings imply that C-BSA based core–shell NCs might be an efficient means of encapsulating, protecting and delivering hydrophobic bioactive compounds for applications in functional foods.

1. Introduction

Encapsulating polyphenols inside food-grade nano-carriers (NCs) is a safe and an efficient way of increasing the oral bioavailability, stability, antimicrobial potential, controlled release and bioaccessibility of phenolic active agents in a specific region of the gastrointestinal tract (GIT) (Huang et al., 2019). Designing functional foods containing natural antimicrobials would maximize the health and therapeutic benefits of the bioactive agents (Lucas-González et al., 2018). However, after ingestion either with food or directly, these macromolecular NCs must first withstand the harsh pH and digestive enzymes in the different sections of the GIT (Minekus et al., 2014). Hence knowledge about the fate and performance of nano-carriers within the human body is essential for ensuring the higher bioaccessibility and targeted release of the encapsulated active agents (Cheng et al., 2019). In this context, physicochemical and structural characteristics of carriers are likely to have a major impact on the fate of these ingested NCs in the GIT. These properties may affect their stability in different regions of GIT including their agglomeration state, interaction with digestive enzymes (amylase, protease, lipase etc.) and with gastrointestinal mucus (McClements, DeLoid et al., 2016; McClements, Saliva-Trujillo et al., 2016). A variety of biobased materials have been tested for this purpose including proteins, carbohydrates and lipids (Penalva et al., 2015).

Chitosan is a biocompatible and biodegradable polysaccharide produced by the deacetylation of chitin. Chitosan has been employed to develop nano-carriers intended for the oral administration due to its cationic nature and resistance to gastric conditions e.g. pH and enzymatic digestion (Braber et al., 2020). In parallel, chitosan demonstrates strong mucoadhesive properties. The nature of the mucus layer depends on the location in the GIT (e.g., mouth, stomach, small intestine and colon). Ingested nano-carriers may adhere to, travel through, or be adsorbed by the mucus layer and GIT

epithelium depending on their physicochemical features thus resulting in improved bioavailability of the encapsulated agent after oral administration (Pauluk et al., 2019).

Carvacrol is a phenolic compound and is a major component of the essential oils (EOs) derived from oregano and thyme. It is generally recognized as safe (GRAS) and demonstrates high antibacterial potential, hence used extensively as a food additive (Martínez-Hernández et al., 2017). However, the application of phenolic compounds i.e. carvacrol is limited due to several factors including low stability and off target release under physiological conditions, high volatility, and low bioavailability in the lower part of the GIT (Engel et al., 2017). These challenges can be effectively improved through encapsulating carvacrol in the biodegradable polysaccharides-based nano-carriers (Assadpour and Jafari, 2019).

Scientific community is pursuing eagerly to decipher the complexity of the fate of NCs in the gastrointestinal (GI) fluids. Many recent studies have reported successful encapsulation of phenolic compounds in pro-tein–polysaccharide based core–shell NCs to enhance their stability and bioaccessibility in GIT (Dai et al., 2018; Foujdar, Bera, & Chopra, 2020; Ren et al., 2019; Wang et al., 2019). All these studies proved that coating of protein-core with oppositely charged polysaccharide-shell, such as chitosan, alginate, and pectin (Hu & McClements, 2015; Huang et al., 2017; Pauluk et al., 2019a) improved their stability by improving steric hindrance between nano-systems while improving their mucoadhesion in the GIT.

However, polysaccharide-core and protein-shell nano-carriers are less explored in terms of their fate in the GIT, especially in the presence of the excipient food. Regarding protein coating on NCs, scientists have focused so far on studying the formation of biological corona on NCs by the proteins present in GI fluids and in food. These recent findings suggest that the formation of protein layer (corona) around NCs can affect their surface characteristics, colloidal stability and mucus inter-action; which influences the release of active agents, bioaccessibility and overall gastrointestinal fate of orally administrated NCs (Cao et al., 2019). In the present study, we have attempted to investigate the effect of GI fluids on protein-coated core–shell NCs in the presence of excipient food.

As reported previously, bovine serum albumin (BSA) - a non- glycosylated anionic protein, can form a shell by adsorbing on the surface of oppositely charged chitosan-core (Fan et al., 2018). This interaction between BSA and chitosan can block the active site for pepsin on BSA. Which in turn reduces the off-target release of active agents by decreasing the gastric digestibility of protein-coated core–shell NCs (Araiza-Calahorra & Sarkar, 2019; Sarkar et al., 2017; Zhao et al., 2019). Recently, it was also observed that BSA coating on polymeric NCs can improve their intracellular penetration in human epithelial cells (Jung & Anvari, 2012; Mariam, Sivakami, & Dongre, 2016).

Therefore, in this study, we have developed core–shell nano-carriers with chitosan (core) and BSA corona (shell), for the encapsulation of carvacrol, their micro-structural and physicochemical characterization were performed during simulated in vitro digestion. For this work, we adopted a standard static in vitro digestion model following INFOGEST recommendations (Brodkorb et al., 2019). These C/BSA core–shell nano-carriers (NCs) were co-digested with skim milk (excipient food) to determine the effect of GI fluids and excipient food on C/BSA core–shell NCs to improve the stability, bioaccessibility, and antibacterial activity of carvacrol during digestion. Thus, these NCs can potentially be employed to develop new food products enriched with phenolic anti-microbial compounds.

2. Materials and methods

2.1. Chemicals

Carvacrol (5-isopropyl-2-methylphenol CAR, ≥98%), medium molecular weight chitosan (C) with 85% degree of deacetylation, tripolyphosphate (TPP), bovine serum albumin (BSA) and fluorescein isothiocyanate (FITC) were purchased from Sigma Aldrich, UK. Phosphate buffer saline (PBS) was purchased from Oxoid-UK. Different digestive enzymes e.g. pepsin, pancreatin bile and all the salts used to prepare simulated electrolyte solutions were also provided by Sigma Aldrich (St Louis, Mo).

2.2. Fabrication of core–shell nano-carriers

For the fabrication of chitosan/bovine serum albumin (C/BSA) based core–shell NCs (CB-NCs), two solutions were prepared. Solution A: 0.3% (w/v) of chitosan was dissolved in 1% (v/v) acetic acid solution. Solu-tion B: 25 mg/mL of BSA in 10 mM NaCl solution and the fabrication was performed as follows.

Step one: Chitosan core nano-systems were prepared by ionic gelation method, 1% TPP (w/v) solution was added dropwise into solution A (chitosan) while stirring. The solution was placed on stirrer for 60 min followed by ultra-sonication for 25 min at 25 kHz. TPP acts as a cross-linker and forms intermolecular interactions with the protonated NH2 group of chitosan (Joshi, Kaur, Khan, Kumar, & Joshi, 2020)

Step two: For the fabrication of BSA-shell on the chitosan-core, nano- carriers (fabricated in step one) were added into BSA solution (solution B) and the solution was placed on stirrer for 30 min at 600 rpm. Synthesized NCs were separated by using centrifugation (Eppendorf-5804R, UK) at 14,000 rpm for 30 min. Supernatant (having unreacted polymer) was discarded and the pellet was washed with phosphate buffer saline (PBS) to get the purified nano-carriers (NCs). Afterwards, NCs were freeze dried and stored for further use. Carvacrol loaded NCs were prepared by dissolving 1 mg/mL of carvacrol in solution A.

2.3. Carvacrol quantification

A gas chromatography-mass spectrometry (GC–MS) method described previously was used to determine the carvacrol concentration in the digesta (Jiménez-Salcedo & Tena, 2017). The oven temperature was programmed in three cycles. In the first cycle, the temperature was maintained at 90 °C for 3 min and then increased to 115 °C at a rate of 3 °C min^{-1}. In the second cycle, temperature was raised to 140 °C with the increase rate of 6 °C min^{-1} and finally, temperature increased at 40°C min^{-1} to 200°C. A calibration curve was set up based on peak areas corresponding to carvacrol concentration of 2.5 to 1000 µg/mL (R2 =0.98). Quantification of carvacrol was performed by comparing content of carvacrol in the digesta with the standard curve obtained from GC–MS.

2.4. Particle diameter, PDI and ζ-potential measurements

The mean particle diameter (Z-average), polydispersity index (PDI), and zeta potential (ζ-potential) of the dispersions of nano-carriers before and after digestion were measured using a dynamic light scattering in-strument (Zetasizer ZS (Malvern), UK). Measuring temperature was 25 ◦C; the fixed angle was 173◦with the refractive index of dispersant (1.33) (Cabezas et al., 2019).

2.5. Morphology of Core-shell NCS

The morphological changes of the C-NCs and CB-NCs containing antimicrobials were investigated using transmission electron microscopy (TEM). To prepare the TEM samples, chitosan (C) nano-systems with BSA-corona were dropped onto the carbon-coated grids and the excess was removed with filter paper. This step was repeated 3 times. Finally, the grids were negatively stained using uranyl acetate solution

(2% w/v) and allowed to dry. TEM images were obtained using a TEM microscope (Jeol-JEM-1230, UK), at an accelerating voltage of 100 kV (Kalhapure et al., 2017)

2.6. *In vitro* simulated digestion

A static *in vitro* gastrointestinal tract (GIT) model was used to study the potential gastrointestinal fate of core–shell nano-carriers and associated bioaccessibility of encapsulated carvacrol. The GIT model described previously (Minekus et al., 2014) was used with slight modifications.

Oral phase: First, electrolyte stock solution (4 mL) representing simulated saliva fluid (SSF) was mixed with the 5 mL of skim milk powder (0.1% nanosystems included) in a 50 mL falcon tube.

Subsequently, 25 µL of 0.3 M CaCl2 and 975 µL of dH2O were added. Lastly, pH was adjusted to 7 and mixture was incubated in a shaking incubator (S1900R, Robus Technologies. UK) at 37 ◦C (80 rpm) for 2mins. Sampling was not performed in the oral phase due to short exposure time of liquids to oral conditions.

Gastric digestion: Electrolyte stock solution (6.4 mL, pH 3) of simulated gastric fluid (SGF) was mixed with the 10 mL oral bolus. Subsequently, 1.6 mL of pepsin with 474 U/mg of enzymatic activity (prepared in SGF) was added, followed by the addition of CaCl2 (5 µL, 0.3 M). Afterwards, pH of the dispersion was adjusted to 3 using 1 M HCl solution. Lastly, to make final ratio of 50:50 (v/v) for oral bolus to SGF, deionized water was added, and the mixture was incubated in a shaking water bath at 37 ◦C at 80 rpm for 60 min. During the gastric phase, samples were taken after regular intervals i.e. 5, 10, 20, 30, 60 min in 1 mL Eppendorf tubes containing NaHCO3 to stop enzymatic activity.

Small intestine phase: Electrolyte stock solution (11 mL) of simulated intestinal fluid (SIF) was added in the remaining sample (17.5 mL) resulting from the gastric phase. Then, 2.5 mL of fresh bile (163.28 mg/ mL) solution was prepared in deionized water, 40 µL of CaCl2 (0.3 M) were included into the above solution and the pH was adjusted to 7 with 1 M NaOH solution. Then, 5 mL of pancreatin solution, containing 0.617 g, that is 4000 U of trypsin activity (prepared in SIF) and 0.79 mL of deionized water was added to make the final ratio of gastric chyme to SIF 50:50 (v/v). Finally, the mixture was placed in the shaking water bath at 37 ◦C (100 rpm) for 1 h.

2.7. Confocal laser scanning microscopy

Confocal laser scanning microscopy (CLSM) was used to characterize the structure of NCs, before and after digestion (LSM710, Carl Zeiss, UK). A 10 × eyepiece and a 60 × oil-immersion objective lens was used. Chitosan polymer was labeled with fluorescein isothiocyanate (FITC) before the fabrication of NCS as described previously (Wang et al., 2017). Labeled C-NCs were observed in the digested samples with or without BSA corona layer (Cheng et al., 2019). Diluted digestion samples (100 µL) having FITC labeled NCs were added into 5 mm deep well of sample holder and covered with a coverslip. Images of the digestion samples were acquired in real-time and fluorescent intensities of un-modified and corona modified NCs were compared.

2.8. Protein digestibility assay: To assess the hydrolysis of BSA-shell on Chitosan-core during digestion

Hydrolysis/digestion of BSA layer on NCs was quantified by the amount of free NH2 groups released during digestion. Free α-amino groups were assessed after reaction with o-phthaldialdehyde (OPA) in micro-titer plates by spectrophotometric assay. All the digestion samples were pretreated with 5% trichloroacetic acid (TCA) to precipitate the insoluble proteins. Samples were centrifuged at 10,000 g for 30 min at room temperature and the supernatant was transferred to new microfuge tubes. Afterwards, 10 µL of each pretreated sample (supernatant) was added in each well and mixed with

200 µL of freshly prepared OPA reagent as described previously (Yi et al., 2016). The reaction was allowed to proceed at room temperature for 15 min, then the absorbance was measured at 340 nm using a microplate spectrophotometer. A calibration curve was made using different concentrations of l-leucine treated with OPA reagent similarly as for samples.

2.9. Bioaccessibility

In vitro bioaccessibility of carvacrol was taken to be the fraction of carvacrol that was solubilized in mixed micelles as described previously (Huang et al., 2017) with slight modifications. The amount of carvacrol released from the various nano-formulations was measured during in vitro gastrointestinal digestion. For this, carvacrol release was measured after the samples were subjected to gastric and small intestine digestion or 0, 5, 10, 20, 30 and 60 min. The samples were then centrifuged at 5000 g for 30 min, and the supernatant was collected and the amount of carvacrol released was quantified with GC–MS (Section 2.7). In vitro bioaccessibility of carvacrol was calculated by using the following equation (1):

$$Bioaccessibility = \frac{Massofsolubilizecarvacrol}{Massofcarvacrolbeforedigestion} \times 100 \qquad (1)$$

This representation of the bioaccessibility depends on the fraction of carvacrol lost due to degradation, as well as the fraction solubilized within the micelle phase after *in vitro* digestion.

3. Results and discussion

3.1. Initial size, shape and surface charge of carvacrol-loaded core–shell NCs

Particle size, zeta potential and PDI are important factors to deter-mine stability as well as in vitro and in vivo behavior of any nano-carrier system for bioactive compounds. An ideal nano-carrier system should be of small size, having high surface charge and low PDI values. PDI is an indicator of dispersion homogeneity. Surface charge and size are important for mucoadhesion and intracellular penetration as well as for stability and controlled release of any encapsulating agent. Fig. 1 demonstrates the mean particle size, ζ-potential and PDI of CAR-loaded C/ BSA core–shell nano-carrier (CAR-CB-NCs). The particle size of void chitosan (C) NCs was 52.4 ±10 nm, which increased to 163 ±4.1 nm after carvacrol encapsulation in C-NCs (CAR- C-NCs). This larger diameter confirms the encapsulation of carvacrol inside the meshwork of C-TPP (tripolyphosphate) NCs. PDI value (0.385) confirmed that C- NCs were not homogeneous in size after carvacrol loading, as PDI >0.3 indicates polydispersity in the systems (Niaz et al., 2018). This aggregation of void and loaded C-NCs can also be seen in TEM images. Similarly, void CB-NCs appeared to be larger in size (203 ±6 nm) than C-NCs (Fig. 1-I). The increase in size is due to the formation of thicker corona layer with oppositely charged protein (BSA) around chitosan- core. These results are in accordance with the previous studies, where larger size particles were observed after the addition of oppositely- charged polymer layer on core nanoparticles (Khan et al., 2019). Mean particle size of C/BSA core–shell NCs was further increased to 445 ±2.7 nm after the addition of carvacrol. This phenomenon might be due to the fact that albumin in its primary structure contains high content of charged amino acids and provides different binding sites for active agents. Hence, BSA allows the electrostatic adsorption of these molecules (active agents) without the requirement of cross-linkers (Elzoghby, Samy, & Elgindy, 2012). Therefore, carvacrol not only got adsorbed on the BSA corona but it was also encapsulated between the chitosan and BSA layer, thus forming a relatively loose structure and resulted in bigger size of particles. This phenomenon also provided the evidence to explain higher encapsulation efficiency (EE %) of carvacrol in CB-NCs (93 ±1%) than C-NCs (68 ±1%).

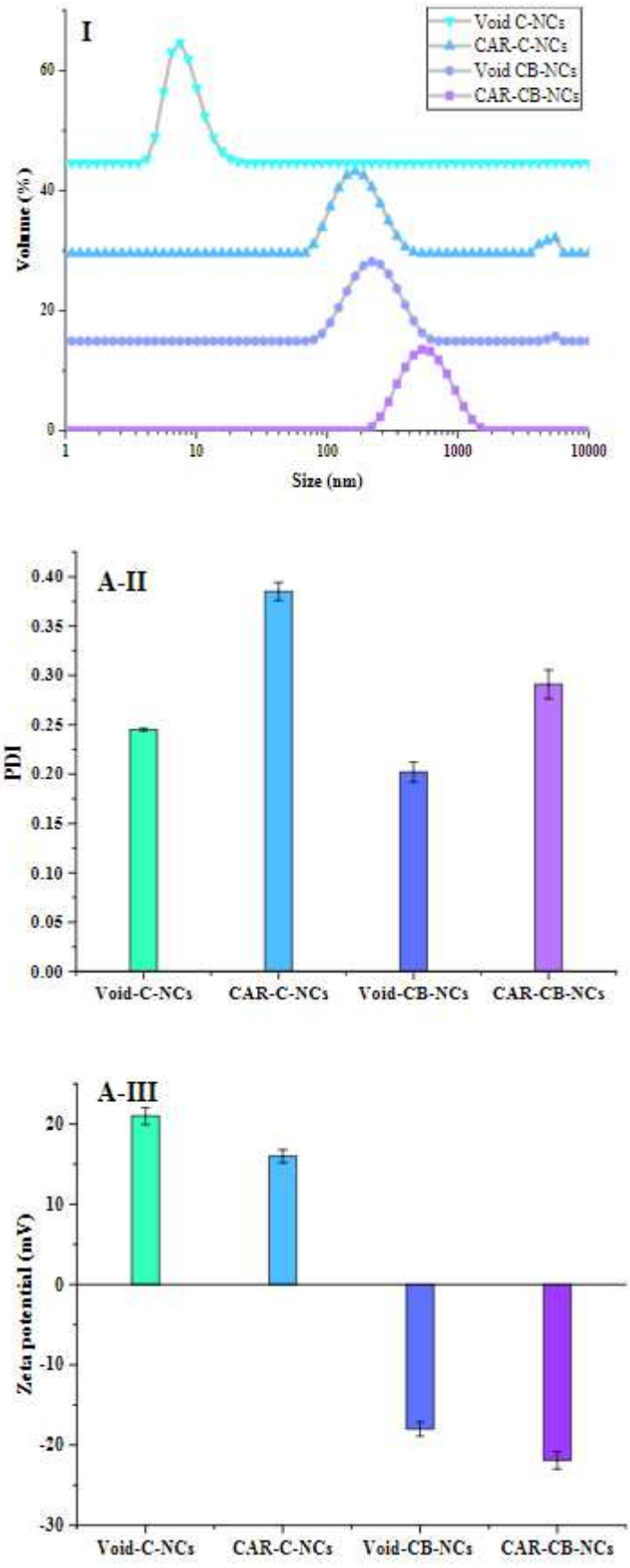

Fig. 1.Initial characterization of core and corona modified chitosan carrier systems based on Zeta-sizer analyses including particle size (I) ζ-potential (II) and PDI (III).

Zeta potential is another important parameter to determine the stability of nanocarrier systems. NCs with higher zeta potential value (either positive or negative) tend to be highly stable particles. Chitosan nanoparticles gave a zeta potential value of +21 ±3.6 mV (Fig. 1-III), implying a positively charged surface of the C-NCs. The zeta potential decreased to +16 ±2 mV for carvacrol-loaded C-NCs. This reflected that the loading of carvacrol reduced the positive surface charge, which might be a result of carvacrol adsorption on the outer-surface of nano- carriers. Similar results were observed for chitosan–TPP nanoparticles encapsulating essential oils (Khan et al., 2019). Interestingly, after coating BSA on C-core, zeta potential values changed from positive (+21 ±3.6 mV) to negative (-18 ±2.7 mV). This shift in ZP of CB-NCs confirmed the formation of anionic BSA shell on cationic chitosan core. ZP further improved after encapsulation of carvacrol in CB-NCs (CAR-CB-NCs) are more stable and BSA protein not only offer stability to the core–shell NCs but also prevents self-aggregation (Mukhopadhyay et al., 2018), which was not observed in case of CAR-C-NCs. The morphology of nano-carriers was assessed by TEM. Individual C- NCs and carvacrol-loaded chitosan nano-carrier systems (CAR-C-NCs) exhibited spherical to oval shape with rough surface morphology (Fig. 2 (I, II)). However, most of the NCs were aggregated. The observations suggested that carvacrol encapsulation did not influence the surface morphology of the C-NCs as no structural changes were observed after carvacrol encapsulation. On the other hand, more homogeneous and smoother surface morphology was observed after the formation of BSA corona on C-NCs, without any aggregation (Fig. 2 (III, IV). BSA coating resulted in an increase in the particle size, which could be explained by the deposition of the negatively charged BSA on the surface of the cationic C-core. Our results are consistent with the previous studies, where coating of the core-NCs with any oppositely charged polymer resulted in bigger size of nano-carriers with improved aggregation sta-bility (Hu & McClements, 2015).

3.2. Influence of simulated gastrointestinal conditions on the stability of core–shell nano-carrier systems

Oral phase: No significant change was observed in the size distribution for both C-NCs and CB-NCs during the oral digestion. Flocculation and coalescence effects have been reported previously during the oral phase, with an increased size ranging from an initial size of 100 nm to>1 μm after the oral phase. This phenomenon has been associated with mucin, a substance that produces strong electrostatic bridges and promotes flocculation (Mun et al., 2017). Mucin and enzyme were not present in the SSF used in the present study, therefore no significant changes in initial size, zeta and PDI were observed during oral phase.

Gastric phase: After oral digestion (short time of 2 min), samples were exposed to the gastric phase (GP). The mean diameter of void C- NCs and CB-NCs increased from initial 52.4 nm and 202 nm to 107 ±3.2 nm and 306 ±5.4 respectively, after just 2 min of exposure to the simulated gastric phase (Fig. 3A-I and II). After 2 min, the mean diameter of the C-NCs suspensions increased greatly (d >300 nm) during gastric phase. Conversely, the increase in particle size of the CB-NCs suspensions during gastric phase was much less (375 ±18 nm) when compared with initial size of CB-NCs. The ζ-potential of the chitosan particles in the gastric “chyme” was highly positive (+33.9 mV) (Fig. 3A-I), which can be attributed to the cationic nature of chitosan below its isoelectric point (pI =6.5) (Koyani et al., 2018). However, ζ-potential (ZP) of C-NCs remained above +30 mV till 10 min of gastric digestion, after that slight decrease in the ZP was observed (+24.1 mV). Conversely, ZP of CB-NCs was highly negative (-40.9 mv), which confirmed the formation of anionic shell of BSA around the core C-NCs. Though continuous decrease in ZP of CB-NCs was observed and it appears to be -25.9 mV at the end of GP. This could be due to the fact that at pH around the isoelectric point (pI =4.7), BSA molecules are in their native and more compact conformation (Rovers et al., 2016). However, BSA had a partially unfolded structure in the pH range from 4 to 2 (pH <pI) and the conformational changes resulted in

reduction of negative ZP values. Secondly, at pH below the isoelectric point of protein (in gastric pH) dissociation of the amino acids starts, which reduce the net negative charge of the CB-NCs. These results coincide with the previous findings, where decrease in pH from 7 to 3 resulted in the reduction of negative ZP on BSA (Li et al., 2016). NCs with ZP of ±10–20 mV, ±20-30 mV and > ±30 mV are considered as relatively stable, moderately stable and highly stable, respectively (Niaz et al., 2018). Hence, CB-NCs remained stable during gastric digestion.

Polydispersity index (PDI) of core and core–shell nano-formulations were ≤0.35 during whole phase of gastric digestion with a slight change indicating mono-dispersity of nano-carriers during gastric digestion. On the contrary, continuous increase in PDI (0.23 to 0.42) with low ZP values (+16.6 to 13.2 mV) from 2 min to 60 min of gastric digestion of carvacrol loaded C-NCs indicated relatively lower stability of the system. Carvacrol loaded CB-NCs remained stable with less PDI (0.34) and higher ZP values (-53.3 to -30.5 mV) than void CB-NCs. It can be inferred that carvacrol provided stability to CB-NCs in the gastric pH, which can be attributed to hydrophobicity of CAR (Flores et al., 2016). Carvacrol molecules could bind to hydrophobic pockets of BSA (Kongot et al., 2018) and thus provide stability to BSA layer (present around C-NCs) against partial hydrolysis by pepsin and conformational changes induced in the acidic gastric conditions.

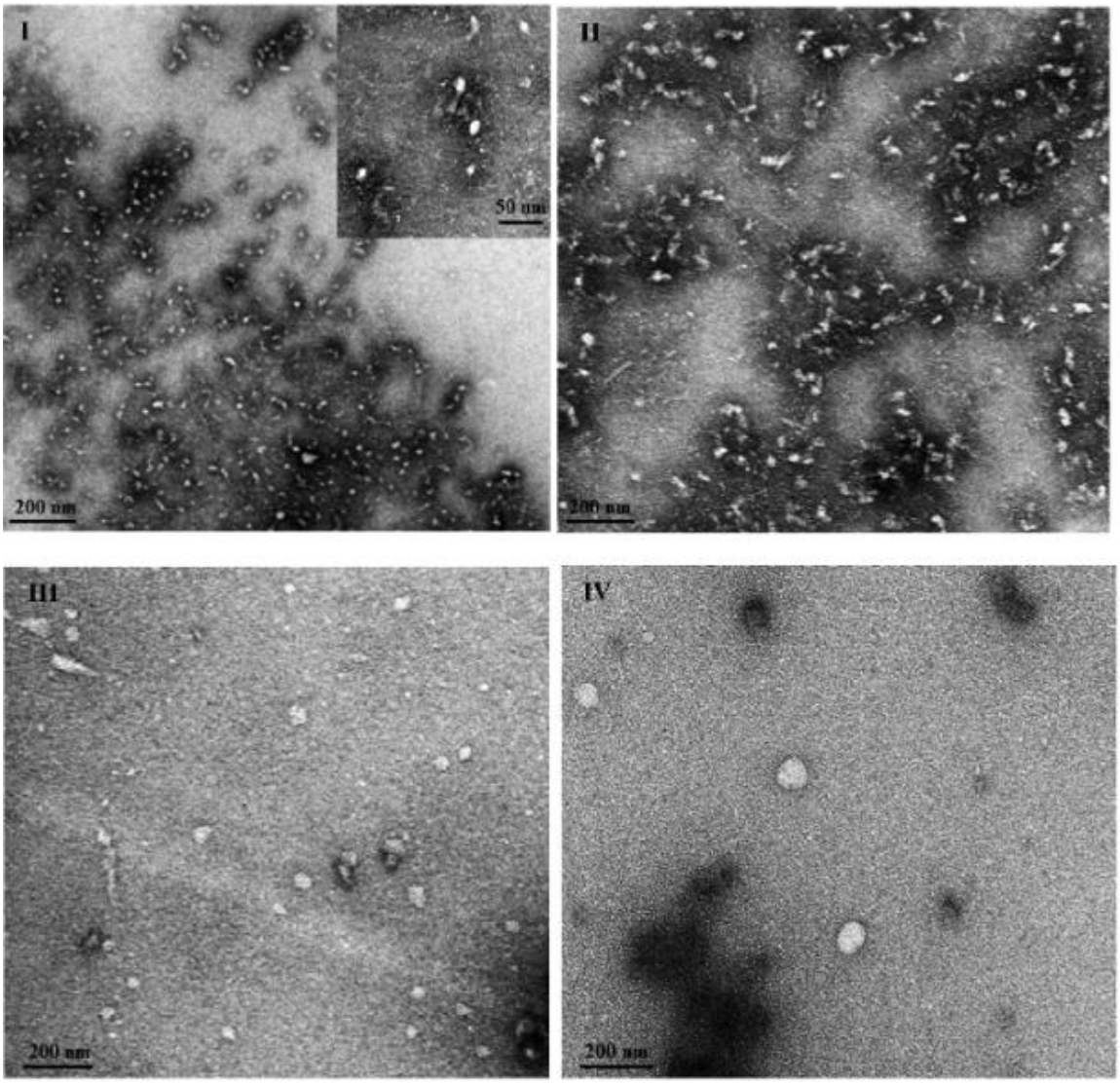

Fig. 2.Transmission electron microscopy of void and active C-NCs (I, II), void and active corona modified nano-carriers (III and IV) respectively.

Intestinal phase: Intestinal digestion was characterized by a decrease in average particle size from 590 ±7 nm to 406 ±9 nm for C- NCs (Fig. 3B-I), with a continuous decrease in ZP to +7.2 mV at the end of intestinal phase of digestion (ID). Possible reason to explain this phenomenon is the deprotonation of chitosan, which starts during the simulated intestinal phase (pH 7) because the pI value of chitosan is around 6.5 (Shin & Kim, 2018). This resulted in less positive charge on chitosan, which led to the dissociation of C-NCs by reducing electrostatic interaction between chitosan and TPP. Furthermore, the ZP of CAR-C- NCs during ID reduced from +10.7 mV to +1.7 mV from 2 to 10 min in SIF, after that ZP became negative and reached to -9.9 mV after 60 min of incubation in SIF (Fig. 3B-II). This alteration could be due to the presence of anionic bile salts in the SIF (Davidov-Pardo et al., 2015). While considering the mean particle size of CAR-C-NCs, a decrease in particle size was observed after 20 min of in vitro intestinal digestion, but subsequently, the particle size reached to 778 ±18 nm after 60 min of ID. The increase in size could be associated to the dissociation due to deprotonation of chitosan in first 20 min, which can permit the release of carvacrol from NCs. Consequently, the undigested chitosan form aggregates after interacting with anionic bile salts, which increased the size of particles. In case of CB-NCs, ZP remained in the range of –22 mV to –18mV for initial 10 min incubation in SIF. However, ZP measurements showed that the CB-NCs became positively charged once again after 10 min, with an even greater charge reduction from gastric phase. ZP values appeared to be +13.2, +12.1 and +10 mV respectively at 20, 30 and 60 min of ID. This indicated complete digestion of BSA layer by intestinal enzymes in initial 10 min, which exposes chitosan-core. Low ZP values also indicated the instability of core C-NCs, which may well be dissociated rapidly in SIF due to pH shock. Nevertheless, continuous increase in particle size of void CB-NCs were observed during whole ID phase that could be an evidence of relatively large protein aggregates in this phase. These aggregates might contain partially digested BSA protein, mixed micelles and undigested vesicles which would be reflected by a high degree of heterogeneity as reflected by the diversity represented in the PDI (>0.3). Conversely, rapid decrease in the particle size with excessive release of anionic species e.g. BSA were evident in the intestinal digestion of carvacrol loaded CB-NCs (CAR-CB-NCs). ZP values changed from negative (-24 mV) to positive (+8.6 mV) after 20 min of ID and particle size reduced from 771 ±8 nm at 2 min to 494 ±13 nm at 60 min of ID, indicating rapid carvacrol release from NCs in this phase. As solubilization of any active agent in SIF occur through interaction with non- polar moieties on the surface of peptides (Yao et al., 2018), thus released molecules of hydrophobic carvacrol will bind to peptides released from the partial digestion of BSA layer (by pancreatin and bile salts), which will reduce the aggregation of peptides. Recently, multiple studies have been published with similar type of data where smaller size-distribution of NCs was observed during intestinal phase of digestion (Huang et al., 2019; Yao et al., 2018).

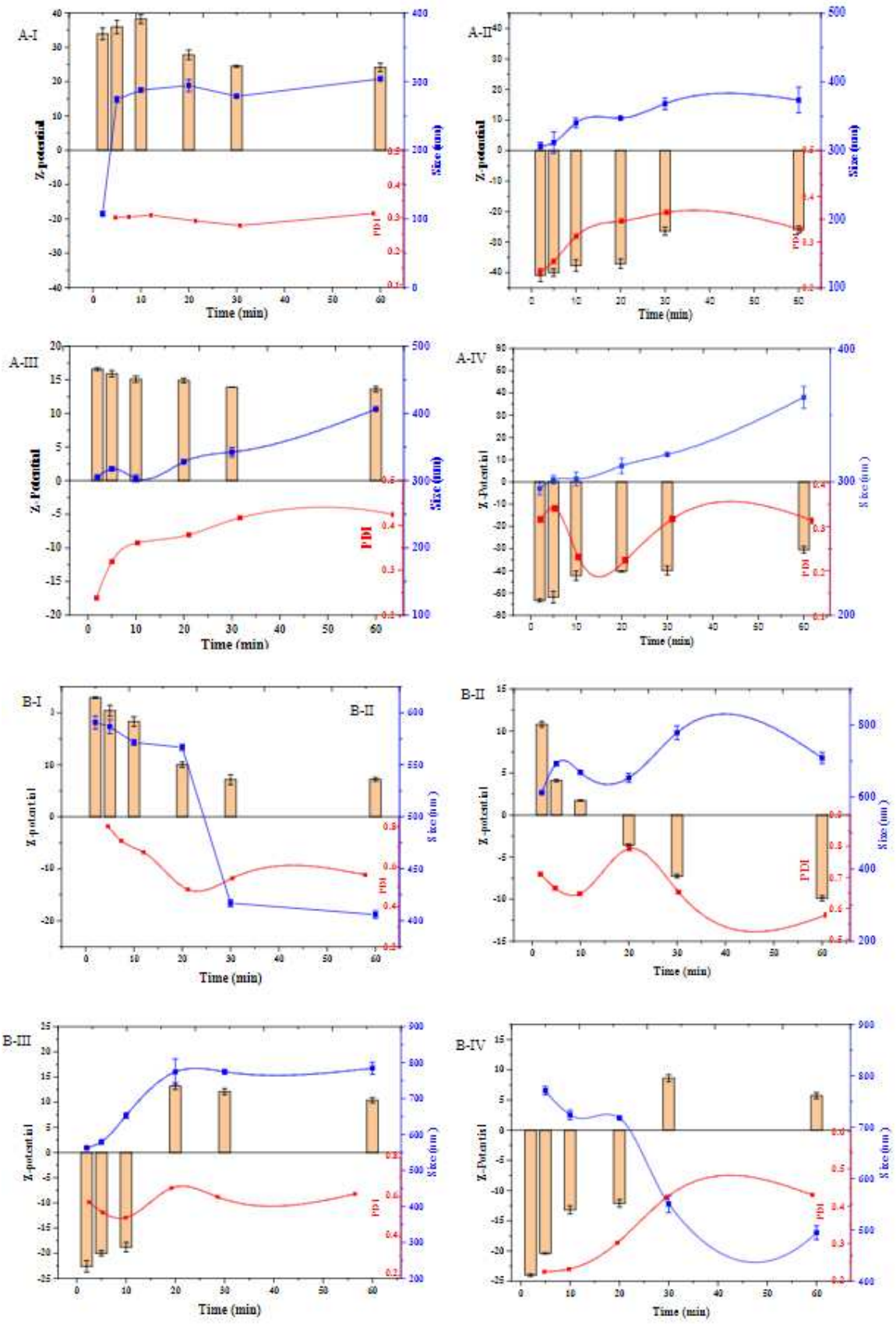

Fig. 3.Characteristic impact on size, PDI and Z-potential under gastric (A) and intestinal digestion (B) phases for void C-NCs (I), carvacrol loaded C-NCs (CAR-C- NCs) (II), void-CB-NCs core–shell nano carriers systems (III), and carvacrol loaded CB-NCs (CAR-CB-NCs) (IV). Mean values (n =3) were plotted and error bars indicate the standard deviations in the data.

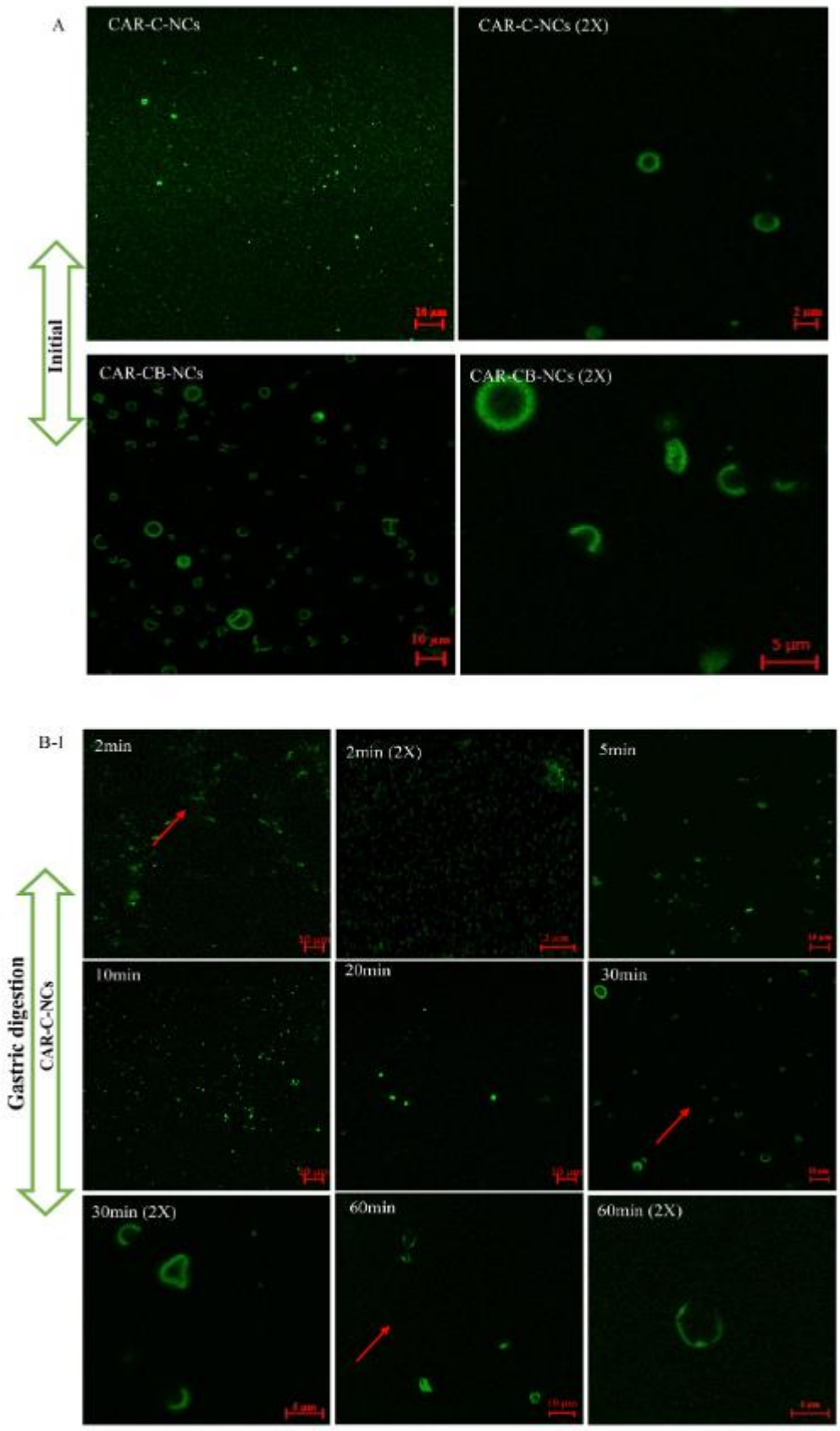

Fig. 4.Influence of simulated gastrointestinal conditions on the structure of core–shell nano-carriers in initial phase (A), CAR-C-NCs (B) and CAR-CB-NCs (C) determined by confocal fluorescence microscopy observed during gastric (I) and intestinal phases (II).

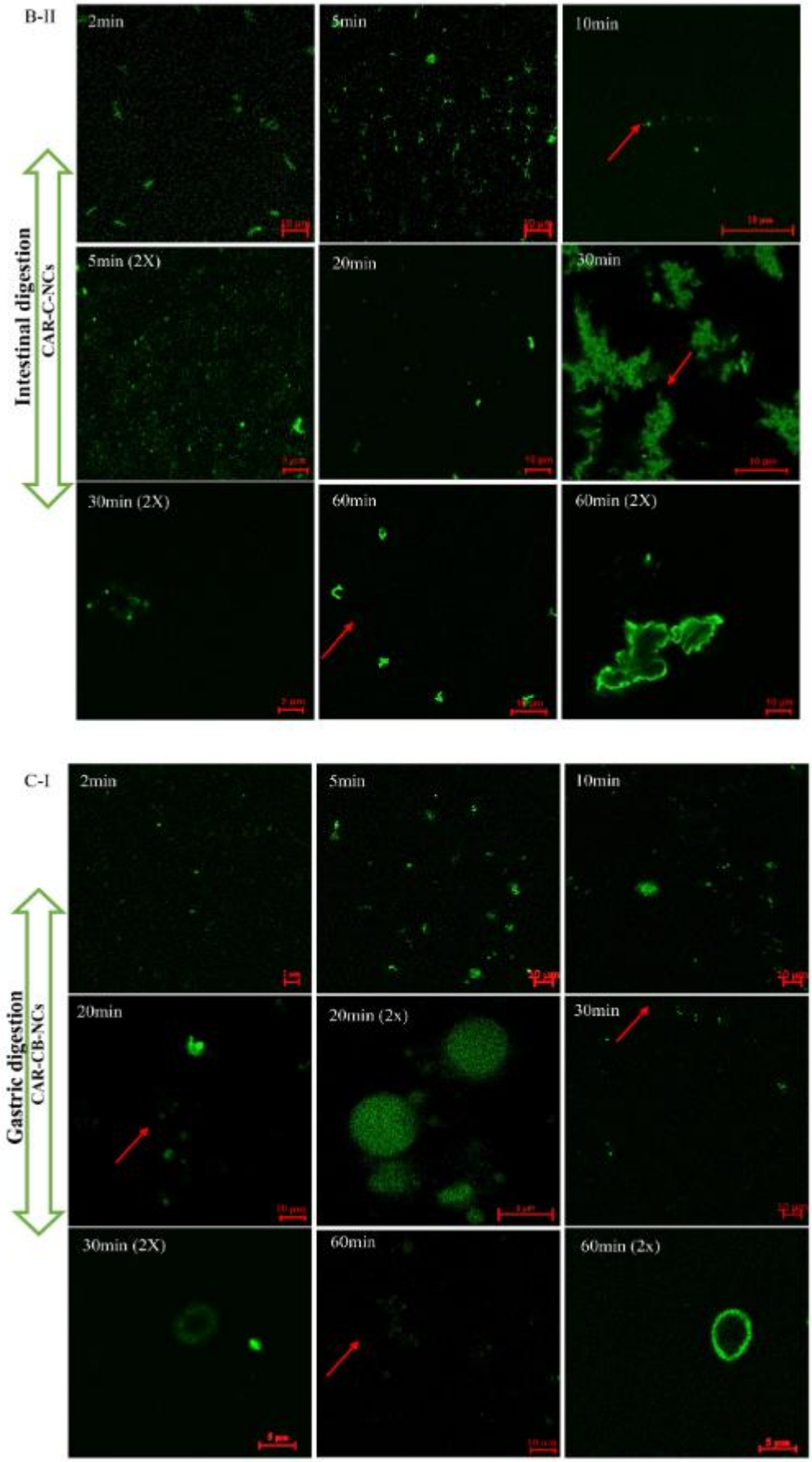

Fig. 4. (*continued*).

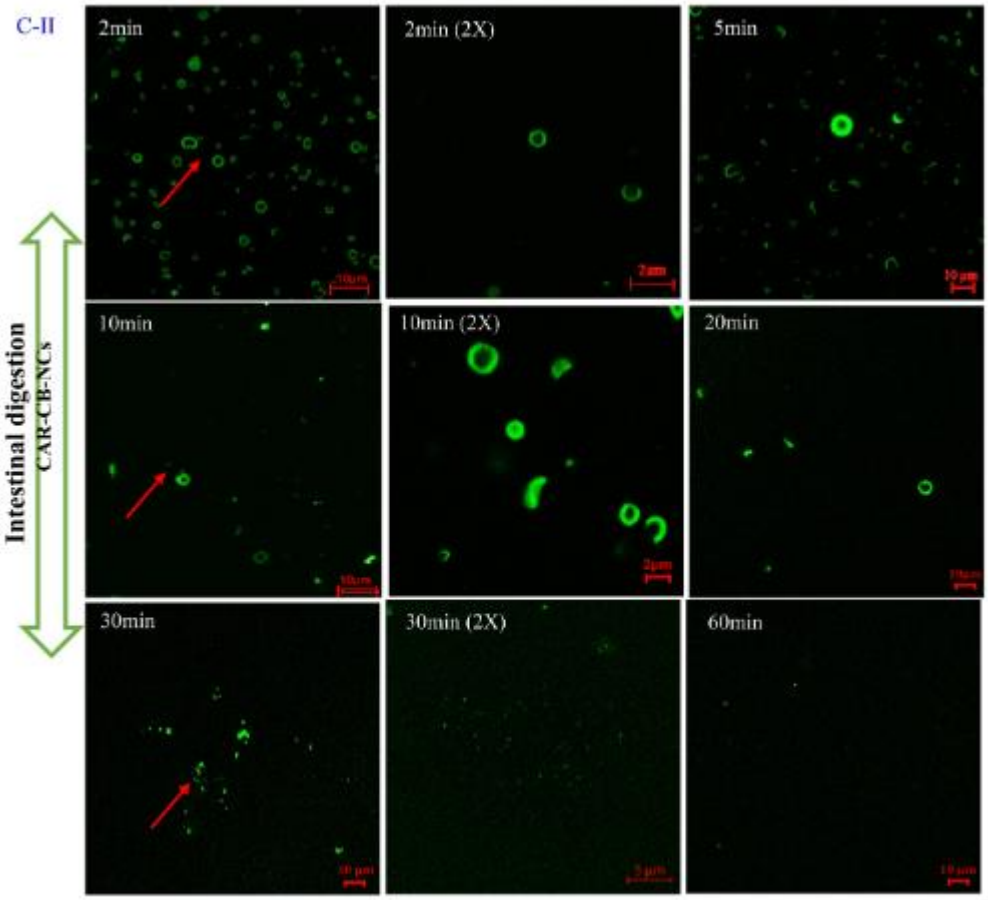

Fig. 4. *(continued).*

3.3. CLSM analysis: Effect of digestion conditions on the structure of core–shell nanosystems

Confocal fluorescence microscopy was performed to observe the effect of gastrointestinal conditions on the microstructure of void and carvacrol loaded NCs (Fig. 4). Fluorescent intensity of NCs before and after the formation BSA shell on core C-NCs were observed. As core- polymer was labeled with FITC for CLSM analysis and it was observed that after the formation of BSA-shell around NCs, fluorescence intensity (FI) was reduced to almost 2500 as compared to core C-NCs which was observed to be in the range of 4000–6000. FI further reduced after carvacrol loading in both unmodified and modified NCs, which indicated that carvacrol was not only encapsulated but also adsorbed on the surface of NCs by hydrophobic interaction (Fig. S2: supplementary data). Confocal microscopy images of loaded C-NCs and CB-NCs before the start of digestion are presented in Fig. 4A, as controls. In confocal microscopy images of C-NCs during gastric digestion (Fig. 4B-I), slight agglomeration between NCs can be seen initially but after 10 min no coalescence was observed. However, unstable structures of C-NCs with relatively larger in size were observed at the end of gastric phase (60min) than initial gastric phase (2 min). Similarly, large agglomerates of undigested polymer after the breakdown of core C-NCs can be seen in the intestinal phase (Fig. 4B-II).

In contrast, when CB-NCs were exposed to SGF (simulated gastric fluid), large flocs of NCs were observed from start till 20 min of the gastric digestion, which can be attributed to the flocculation induced by BSA-shell of NCs (Fan et al., 2018). These effects may result from dilution or changes in the aqueous phase composition in the SGF; such as changes in pH, ionic strength, and enzyme activity (Liu et al., 2018). However, CAR-CB-NCs remained in stable configuration at the end of GP (Fig. 4C-I). When the aggregated nano-carriers were exposed to the intestinal phase, they dissociated, though particle

size of these NCs was relatively large but they were present in more monodisperse and stable configuration (Fig. 4C-II) than core C-NCs. Chitosan NCs are characterized by a net positive surface charge at pH 7 (Rampino et al., 2016). Conversely, at this pH (above the pI of BSA), BSA attained a highly negative charge which promoted the formation of protein-shell around chitosan (Cai & Lapitsky, 2017). This resulted in an improved electro-static interaction between C and BSA. These observations are consistent with the Z-potential values determined by electrophoretic mobility as discussed earlier. Dai et al. found that curcumin-loaded zein nano-systems formed extensive aggregations in the simulated gastric juices. However, the size reduction of NCs when submitted to SIF was attributed to the bile salts, which has strong emulsifying ability (Dai, Li, et al., 2018).

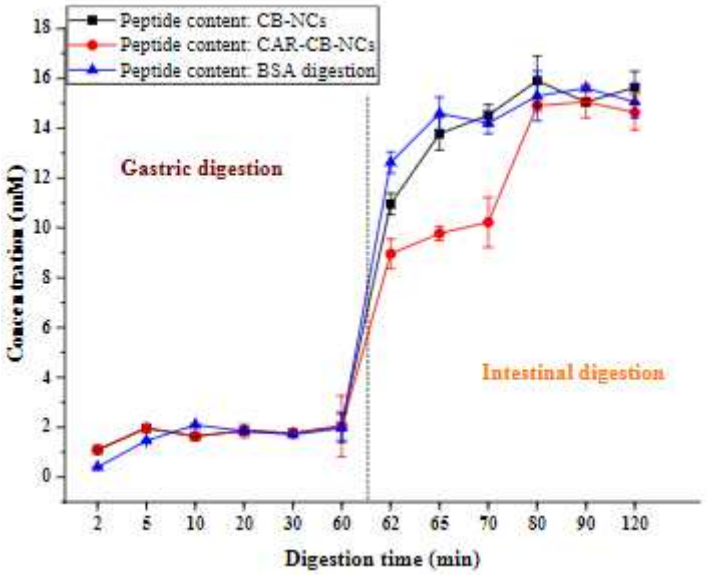

Fig. 5. Quantification of digested BSA-shell during *in vitro* gastrointestinal digestion performed by OPA assay. Leucine standard curve was used to quantify the digestion of protein-layer from void and carvacrol loaded C-BSA core–shell NCs. BSA without nanostructure was used as control.

3.4. Protein digestibility determination by OPA assay

Digestibility of protein-shell in the core–shell NCs remains below 2 mM during whole gastric digestion in all formulations. Subsequently, protein digestibility of void CB-NCs formulations obtained after intestinal digestion increased to values ranging from 9 mM to 16 mM, which was the same as the digestion of free BSA protein without any nanostructure formation during initial ID (Fig. 5). As observed previously, the presence of bile salts in intestinal digestion phase increases hydrolysis of proteins (Giteru et al., 2020). Rate of protein digestion was reduced significantly in case of carvacrol loaded CB-NCs during initial 10 min of intestinal digestion. A possible explanation for the increased protection of BSA-shell after carvacrol addition might be related to the entrapment of carvacrol (present between C-core and BSA-shell) in the hydrophobic cavities of BSA, which blocked the active cleavage sites of BSA and thus presented limited access for intestinal enzymes to cleave the different sites of BSA-shell. These results confirmed that CAR-CB- NCs remained more stable in the intestinal phase.

3.5. Gastrointestinal fate of core–shell nano-antimicrobials and bioaccessibility of carvacrol

To have any beneficial antimicrobial effects, it is important that encapsulated active agents are released in the GIT at target site. In this study, *in vitro* bioaccessibility of carvacrol was determined by measuring its percentage release into the gastrointestinal fluids at different stages in the simulated

GIT conditions. In vitro, bioaccessibility values of carvacrol were compared in three different formulations i.e. free carvacrol, encapsulated in C and in core–shell NCs.

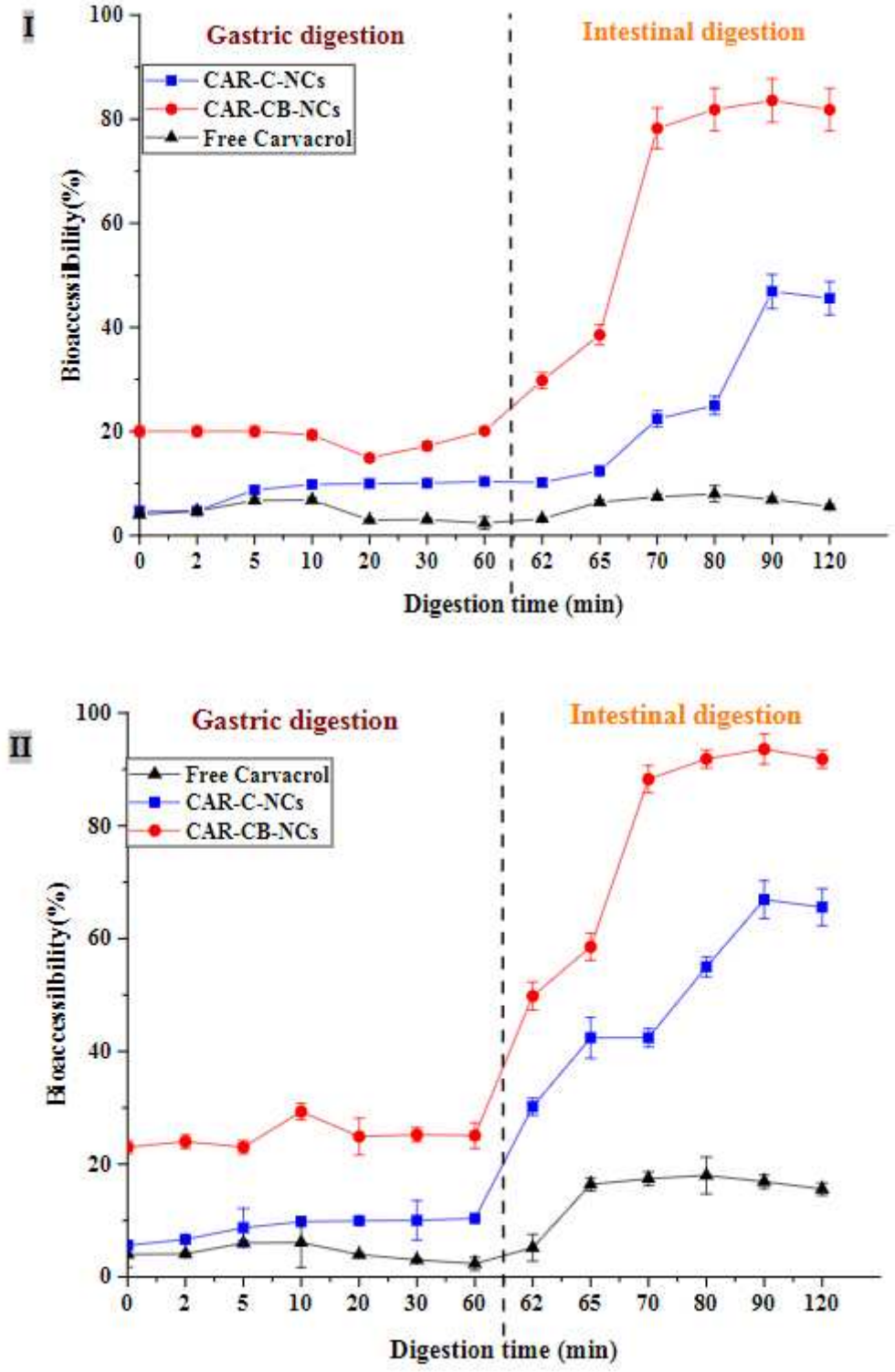

Fig. 6.Bioaccessibility of free carvacrol and carvacrol-loaded in corona modified nano-carriers (CAR-CB-NCs) and C-NCs without BSA-corona (CAR-C-NCs) during stimulated gastric and small intestinal digestion without excipient (I) and with excipient food (Skim milk) (II).

High levels of carvacrol release in the simulated gastric fluids at zero digestion time indicated significantly higher solubility of the carvacrol encapsulated in CB-NCs (CAR-CB-NCs) than C-core NCs (Fig. 6-I). Hence, core–shell NCs provided relatively high surface area exposed to the gastric fluids, therefore, carvacrol release from CAR-CB-NCs was slightly higher than CAR-C-NCs in gastric phase. Similarly, when moved to intestinal stage, these coronae modified NCs demonstrate much more rapid release probably due to the presence of bile salts and enzymes in the SIF, which formed micelles or complexes that solubilized the released carvacrol. Similar results were observed by Huang et al., where encapsulation of resveratrol in zein/pectin core–shell nanoparticles improves its solubility and bioaccessibility during gastrointestinal digestion (Huang et al., 2019).

The amount of carvacrol released at the end of the gastric phase was appreciably higher for the coated nano-systems (22 ±1.4%) than for C- NCs (10.9 ±1.1%), and a similar trend was observed in the small intestine phase. The higher bioaccessibility of the encapsulated carvacrol could be due to the generation of soluble peptides from the digestion of BSA-corona present on the NCs (as we can see in the previous section, large amount of peptides were released from the hydrolysis of BSA- corona in the intestinal phase than gastric phase), which can bind to carvacrol and increase its solubility in the intestinal phase (Chen et al., 2018). The solubilized material can then be transported through gastrointestinal lumen and diffuse through the mucus layer, until it reaches the epithelial cells where it can be absorbed (Yao et al., 2018). Furthermore, the relatively higher surface area of the NCs may have led to a more rapid release of the carvacrol into the gastrointestinal fluids (Esfanjani & Jafari, 2016), which resulted in an improved bioaccessibility of the encapsulated agent.

Overall in vitro bioaccessibility of the encapsulated carvacrol was improved in the presence of the excipient food i.e. skim milk (Fig. 6-II), when compared to the simulated digestion without excipient. The bio-accessibility index revealed that the liberation of carvacrol from CB-NCs was improved up to 91 ±4.9% when digested with skim milk, which was around 80 ±3.1% without excipient. Similarly, carvacrol release increased almost 40% from C-NCs with excipient. This may have occurred because the milk proteins could possibly have better free radical scavenging or iron chelation properties, which protected the released carvacrol from chemical degradation (Chen et al., 2018). Secondly, solubilization of the carvacrol was improved after interacting with the hydrophobic interiors of the mixed micelles formed by lipid digestion present in excipient milk (McClements, DeLoid et al., 2016; McClements, Saliva-Trujillo et al., 2016). Additionally, interactions between the peptides generated by the proteolysis of skim milk may have also contributed to micellization, which favored the solubilization of carvacrol and thus resulted in its improved bioaccessibility. From these results, we can conclude that C/BSA core–shell NCs led to an appreciable increase for *in vitro* bioaccessibility of antimicrobial phenolic compound, which further improved in the presence of the excipient food. Thus, our results suggest that food matrix has profound effect on micellization of the released carvacrol from NCs during gastrointestinal digestion.

4. Conclusion

In this work, chitosan and BSA-based core–shell NCs were fabricated for the effective encapsulation and gastrointestinal stability of carvacrol. Zeta potential values of C-NCs reversed from positive to negative charge with the formation of anionic BSA-shell. Protein-corona reduced the aggregation of nano-carriers by improving the steric hindrance. Furthermore, significant improvement of carvacrol bioaccessibility in GIT environment was also provided by core–shell nano-systems. These modified nano-carriers have the potential for wide-spread applications of the studied natural antimicrobial (as well as antioxidant) for extending the shelf-life, reducing the spoilage, and better ensuring the safety of a variety of food products. However, further investigations are required to assess the effects of

biological corona formed by different excipient proteins on the digestibility and stability of the nano-antimicrobials.

CRediT authorship contribution statement

Taskeen Niaz: Conceptualization, Methodology, Investigation, Writing - original draft. Muhammad Imran: Supervision, Conceptualization, Validation, Resources, Writing - review & editing, Project administration. Alan Mackie: Supervision, Conceptualization, Validation, Resources, Writing - review & editing, Project administration, Funding acquisition.

Declaration of Competing Interest

The authors declare that they have no known competing financial interests or personal relationships that could have appeared to influence the work reported in this paper.

Acknowledgement

The authors are grateful to Higher Education Commission (HEC), Pakistan for funding during IRSIP Vide Letter No. 1-8/HEC/HRD/2017/ 8168 and for the National Research Program for Universities (NRPU) Vide Grant No. 20-4260/R&D/HEC/14/127.

Appendix A. Supplementary data

Supplementary data to this article can be found online at https://doi.org/10.1016/j.foodchem.2021.129505.

References

Braber, N. V., Vergara, L. D., Rossi, Y., Aminahuel, C., Mauri, A., Cavaglieri, L., & Montenegro, M. (2020). Effect of microencapsulation in whey protein and water- soluble chitosan derivative on the viability of the probiotic Kluyveromyces marxianus VM004 during storage and in simulated gastrointestinal conditions. LWT, 118, Article 108844.

Cabezas, D. M., Pascual, G. N., Wagner, J. R., & Palazolo, G. G. (2019). Nanoparticles assembled from mixtures of whey protein isolate and soluble soybean polysaccharides. Structure, interfacial behavior and application on emulsions subjected to freeze-thawing. Food Hydrocolloids, 95, 445–453.

Cai, Y., & Lapitsky, Y. (2017). Analysis of chitosan/tripolyphosphate micro and nanogel yields is key to understanding their protein uptake performance. Journal of colloid and interface science, 494, 242–254.

Cao, X., Han, Y., Li, F., Li, Z., McClements, D. J., He, L., Decker, E. A., Xing, B., & Xiao, H. (2019). Impact of protein-nanoparticle interactions on gastrointestinal fate of ingested nanoparticles: Not just simple protein corona effects. NanoImpact, 13, 37–43.

Chen, X., McClements, D. J., Zhu, Y., Chen, Y., Zou, L., Liu, W., ... Liu, C. (2018). Enhancement of the solubility, stability and bioaccessibility of quercetin using protein-based excipient emulsions. Food Research International, 114, 30–37. https:// doi.org/10.1016/j.foodres.2018.07.062.

Cheng, C. J., Ferruzzi, M., & Jones, O. G. (2019). Fate of lutein-containing zein nanoparticles following simulated gastric and intestinal digestion. Food Hydrocolloids, 87, 229–236. https://doi.org/10.1016/j.foodhyd.2018.08.013.

Dai, L., Li, R., Wei, Y., Sun, C., Mao, L., & Gao, Y. (2018). Fabrication of zein and rhamnolipid complex nanoparticles to enhance the stability and in vitro release of curcumin. Food Hydrocolloids, 77, 617–628.

Dai, L., Wei, Y., Sun, C., Mao, L., McClements, D. J., & Gao, Y. (2018). Development of protein-polysaccharide-surfactant ternary complex particles as delivery vehicles for curcumin. Food Hydrocolloids, 85, 75–85.

Davidov-Pardo, G., P´erez-Ciordia, S., Marín-Arroyo, M. R., & McClements, D. J. (2015). Improving resveratrol bioaccessibility using biopolymer nanoparticles and complexes: Impact of protein–carbohydrate maillard conjugation. Journal of agricultural and food chemistry, 63(15), 3915–3923. Elzoghby, A. O., Samy, W. M., & Elgindy, N. A. (2012). Albumin-based nanoparticles as potential controlled release drug delivery systems. Journal of Controlled Release, 157 (2), 168–182. https://doi.org/10.1016/j.jconrel.2011.07.031.

Engel, J. B., Heckler, C., Tondo, E. C., Daroit, D. J., & da Silva Malheiros, P. (2017). Antimicrobial activity of free and liposome-encapsulated thymol and carvacrol against Salmonella and Staphylococcus aureus adhered to stainless steel. International Journal of Food Microbiology, 252, 18–23. https://doi.org/10.1016/j. ijfoodmicro.2017.04.003.

Esfanjani, A. F., & Jafari, S. M. (2016). Biopolymer nano-particles and natural nano- carriers for nano-encapsulation of phenolic compounds. Colloids and Surfaces B: Biointerfaces, 146, 532–543.

Fan, Y., Liu, Y., Gao, L., Zhang, Y., & Yi, J. (2018). Improved chemical stability and cellular antioxidant activity of resveratrol in zein nanoparticle with bovine serum albumin-caffeic acid conjugate. Food Chemistry, 261, 283–291. https://doi.org/ 10.1016/j.foodchem.2018.04.055.

Flores, Z., San Martín, D., Villalobos-Carvajal, R., Tabilo-Munizaga, G., Osorio, F., & Leiva-Vega, J. (2016). Physicochemical characterization of chitosan-based coating- forming emulsions: Effect of homogenization method and carvacrol content. Food Hydrocolloids, 61, 851–857. https://doi.org/10.1016/j.foodhyd.2016.07.007.

Foujdar, R., Bera, M. B., & Chopra, H. K. (2020). Phenolic nanoconjugates and its application in food. In Biopolymer-Based Formulations (pp. 751–780). Elsevier.

Giteru, S. G., Cridge, B., Oey, I., Ali, A., & Altermann, E. (2020). In-vitro degradation and toxicological assessment of pulsed electric fields crosslinked zein-chitosan-poly(vinylalcohol) biopolymeric films. Food and Chemical Toxicology, 135, 111048. https://doi. org/10.1016/j.fct.2019.111048.

Hu, K., & McClements, D. J. (2015). Fabrication of biopolymer nanoparticles by antisolvent precipitation and electrostatic deposition: Zein-alginate core/shell nanoparticles. Food Hydrocolloids, 44, 101–108. https://doi.org/10.1016/j. foodhyd.2014.09.015.

Huang, X., Dai, Y., Cai, J., Zhong, N., Xiao, H., McClements, D. J., & Hu, K. (2017). Resveratrol encapsulation in core-shell biopolymer nanoparticles: Impact on antioxidant and anticancer activities. Food Hydrocolloids, 64, 157–165.

Huang, X., Liu, Y., Zou, Y., Liang, X., Peng, Y., McClements, D. J., & Hu, K. (2019). Encapsulation of resveratrol in zein/pectin core-shell nanoparticles: Stability, bioaccessibility, and antioxidant capacity after simulated gastrointestinal digestion. Food Hydrocolloids, 93, 261–269. https://doi.org/10.1016/j.foodhyd.2019.02.039.

Joshi, B., Kaur, J., Khan, E., Kumar, A., & Joshi, A. (2020). Ultrasonic atomizer driven development of doxorubicin-chitosan nanoparticles as anticancer therapeutics: Evaluation of anionic cross-linkers. Journal of Drug Delivery Science and Technology, 57, 101618. https://doi.org/10.1016/j.jddst.2020.101618.

Jung, B., & Anvari, B. (2012). Synthesis and characterization of bovine serum albumin- coated nanocapsules loaded with indocyanine green as potential multifunctional nanoconstructs. Biotechnology progress, 28(2), 533–539.

Jiménez-Salcedo, M., & Tena, M. T. (2017). Determination of cinnamaldehyde, carvacrol and thymol in feedstuff additives by pressurized liquid extraction followed by gas chromatography–mass spectrometry. Journal of Chromatography A, 1487, 14–21.

Kalhapure, R. S., Jadhav, M., Rambharose, S., Mocktar, C., Singh, S., Renukuntla, J., & Govender, T. (2017). pH-responsive chitosan nanoparticles from a novel twin-chain anionic amphiphile for controlled and targeted delivery of vancomycin. Colloids and Surfaces B: Biointerfaces, 158, 650–657. https://doi.org/10.1016/j. colsurfb.2017.07.049.

Khan, M. A., Yue, C., Fang, Z., Hu, S., Cheng, H., Bakry, A. M., & Liang, L. (2019). Alginate/chitosan-coated zein nanoparticles for the delivery of resveratrol. Journal of Food Engineering, 258, 45–53. https://doi.org/10.1016/j.jfoodeng.2019.04.010.

Kongot, M., Maurya, N., Dohare, N., Parray, M.u. D., Maurya, J. K., Kumar, A., & Patel, R. (2018). Enthalpy-driven interaction between dihydropyrimidine compound and bovine serum albumin: A spectroscopic and computational approach. Journal of Biomolecular Structure and Dynamics, 36(5), 1161–1170.

Koyani, R. D., Andrade, M., Quester, K., Gayťan, P., Huerta-Saquero, A., & Vazquez- Duhalt, R. (2018). Surface modification of protein enhances encapsulation in chitosan nanoparticles. Applied Nanoscience, 8(5), 1197–1203.

Li, R., Wu, Z., Wangb, Y., Ding, L., & Wang, Y. (2016). Role of pH-induced structural change in protein aggregation in foam fractionation of bovine serum albumin. Biotechnology Reports, 9, 46–52.

Liu, F., Ma, D., Luo, X., Zhang, Z., He, L., Gao, Y., & McClements, D. J. (2018). Fabrication and characterization of protein-phenolic conjugate nanoparticles for co- delivery of curcumin and resveratrol. Food Hydrocolloids, 79, 450–461. https://doi. org/10.1016/j.foodhyd.2018.01.017.

Lucas-González, R., Viuda-Martos, M., Pérez-Alvarez, J. A., & Fernández-López, J. (2018). In vitro digestion models suitable for foods: Opportunities for new fields of application and challenges. Food Research International, 107, 423–436. https://doi. org/10.1016/j.foodres.2018.02.055.

Mariam, J., Sivakami, S., & Dongre, P. M. (2016). Albumin corona on nanoparticles–a strategic approach in drug delivery. Drug delivery, 23(8), 2668–2676.

McClements, D. J., DeLoid, G., Pyrgiotakis, G., Shatkin, J. A., Xiao, H., & Demokritou, P. (2016). The role of the food matrix and gastrointestinal tract in the assessment of biological properties of ingested engineered nanomaterials (iENMs): State of the science and knowledge gaps. NanoImpact, 3–4, 47–57. https://doi.org/10.1016/j. impact.2016.10.002.

McClements, D. J., Saliva-Trujillo, L., Zhang, R., Zhang, Z., Zou, L., Yao, M., & Xiao, H. (2016). Boosting the bioavailability of hydrophobic nutrients, vitamins, and nutraceuticals in natural products using excipient emulsions. Food Research International, 88, 140–152.

Minekus, M., Alminger, M., Alvito, P., Ballance, S., Bohn, T., Bourlieu, C., Brodkorb, A. (2014). A standardised static in vitro digestion method suitable for food–an international consensus. Food & function, 5(6), 1113–1124.

Mukhopadhyay, P., Maity, S., Mandal, S., Chakraborti, A. S., Prajapati, A. K., & Kundu, P. P. (2018). Preparation, characterization and in vivo evaluation of pH sensitive, safe quercetin-succinylated chitosan-alginate core-shell-corona nanoparticle for diabetes treatment. Carbohydrate Polymers, 182, 42–51. https://doi. org/10.1016/j.carbpol.2017.10.098.

Mun, S., Kim, J., McClements, D. J., Kim, Y.-R., & Choi, Y. (2017). Fluorescence imaging of spatial location of lipids and proteins during digestion of protein-stabilized oil-in- water emulsions: A simulated gastrointestinal tract study. Food Chemistry, 219, 297–303.

Niaz, T., Shabbir, S., Noor, T., Abbasi, R., Raza, Z. A., & Imran, M. (2018). Polyelectrolyte multicomponent colloidosomes loaded with nisin Z for enhanced antimicrobial activity against foodborne resistant pathogens. Frontiers in microbiology, 8, 2700.

Pauluk, D., Padilha, A. K., Khalil, N. M., & Mainardes, R. M. (2019). Chitosan-coated zein nanoparticles for oral delivery of resveratrol: Formation, characterization, stability, mucoadhesive properties and antioxidant activity. Food Hydrocolloids, 94, 411–417.

Penalva, R., Esparza, I., Larraneta, E., González-Navarro, C. J., Gamazo, C., & Irache, J. M. (2015). Zein-based nanoparticles improve the oral bioavailability of resveratrol and its anti-inflammatory effects in a mouse model of endotoxic shock. Journal of Agricultural and Food Chemistry, 63(23), 5603–5611.

Rampino, A., Borgogna, M., Bellich, B., Blasi, P., Virgilio, F., & Cesáro, A. (2016). Chitosan-pectin hybrid nanoparticles prepared by coating and blending techniques. European Journal of Pharmaceutical Sciences, 84, 37–45.

Rovers, T. A. M., Sala, G., van der Linden, E., & Meinders, M. B. J. (2016). Temperature is key to yield and stability of BSA stabilized microbubbles. Food Hydrocolloids, 52, 106–115. https://doi.org/10.1016/j.foodhyd.2015.05.038.

Shin, G. H., & Kim, J. T. (2018). Observation of chitosan coated lipid nanoparticles with different lipid compositions under simulated in vitro digestion system. Food Hydrocolloids, 84, 146–153. https://doi.org/10.1016/j.foodhyd.2018.05.052.

Wang, Q., Zhao, Y., Guan, L., Zhang, Y., Dang, Q., Dong, P., Li, J., & Liang, X. (2017). Preparation of astaxanthin-loaded DNA/chitosan nanoparticles for improved cellular uptake and antioxidation capability. Food Chemistry, 227, 9–15. https://doi.org/ 10.1016/j.foodchem.2017.01.081.

Yao, K., Chen, W., Song, F., McClements, D. J., & Hu, K. (2018). Tailoring zein nanoparticle functionality using biopolymer coatings: Impact on curcumin bioaccessibility and antioxidant capacity under simulated gastrointestinal conditions. Food Hydrocolloids, 79, 262–272. https://doi.org/10.1016/j. foodhyd.2017.12.029.

Yi, L., Van Boekel, M. A. J. S., Boeren, S., & Lakemond, C. M. M. (2016). Protein identification and in vitro digestion of fractions from Tenebrio molitor. European Food Research and Technology, 242(8), 1285–1297. https://doi.org/10.1007/s00217- 015-2632-6